

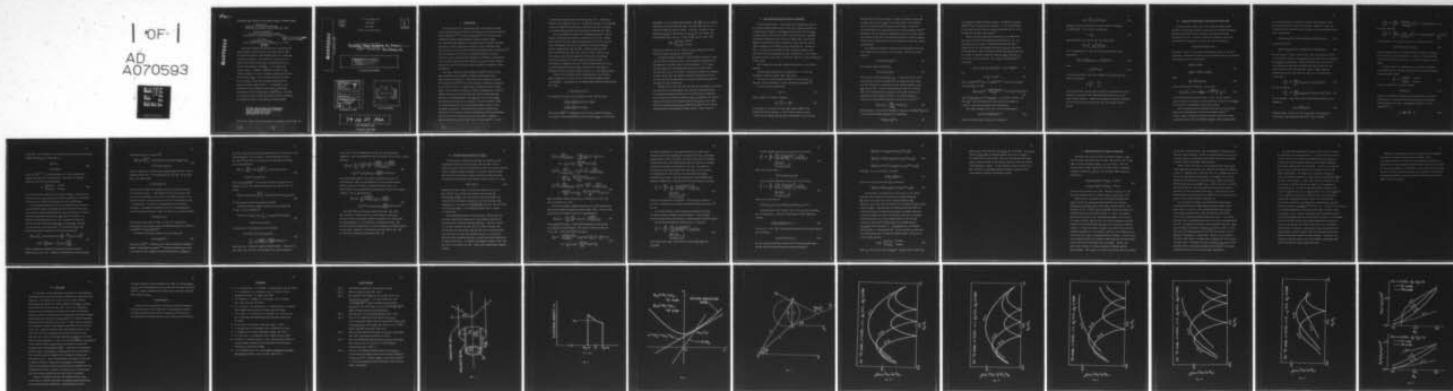
AD-A070 593

MARYLAND UNIV COLLEGE PARK DEPT OF PHYSICS AND ASTRONOMY F/6 20/5
CYCLOTRON MASER INSTABILITY FOR GENERAL MAGNETIC HARMONIC NUMBE--ETC(U)
1975 H UHM, R C DAVIDSON, K R CHU N00014-75-C-0309

UNCLASSIFIED

NL

| OF |
AD
A070593



END
DATE
FILMED
8-79
DDC

Code 6702

CYCLOTRON MASER INSTABILITY FOR GENERAL MAGNETIC HARMONIC NUMBER

Hwan-sup Uhm
Department of Physics and Astronomy
University of Maryland, College Park, Md. 20742

Ronald C. Davidson*
Division of Magnetic Fusion Energy
Department of Energy, Washington, D. C. 20545

K. R. Chu
Plasma Physics Division
Naval Research Laboratory, Washington, D. C. 20375

APPROVED FOR PUBLIC RELEASE
DISTRIBUTION UNLIMITED

1975

This paper examines the cyclotron maser instability for general magnetic harmonic number transverse electric (TE) and transverse magnetic (TM) waveguide modes in a conducting cylinder of radius R_c . The analysis is carried out for a hollow electron beam (radius R_0) propagating parallel to a uniform axial magnetic field $B_0 \hat{e}_z$. It is assumed that $v/\gamma_0 \ll 1$, where v is Budker's parameter and $\gamma_0 mc^2$ is the electron energy in a frame of reference moving with the beam axial velocity $\beta_b c \hat{e}_z$. One of the most important features of the analysis is that the instability growth rate for magnetic harmonic numbers $s=2,3,\dots$ is comparable to the growth rate of the fundamental ($s=1$) mode, particularly for moderate electron energy [$\beta_0 = (1 - 1/\gamma_0^2)^{1/2} \gtrsim 0.4$]. Moreover, it is shown that the instability growth rate can be maximized by appropriate choice of the geometric parameter R_0/R_c .

ADA070593

Work on this report was supported
by ONR Contract N00014-75-C-0309
and/or N00014-67-A-0239
monitored by NRL 6702.

* On leave of absence from the University of Maryland, College Park, Md.

79 06 27 302

ADA 070593

DDC ACCESSION NUMBER



LEVEL

DDC PROCESSING DATA

PHOTOGRAPH

THIS SHEET



INVENTORY

RETURN TO DDA-2 FOR FILE

Cyclotron Maser Instability for General - - - -

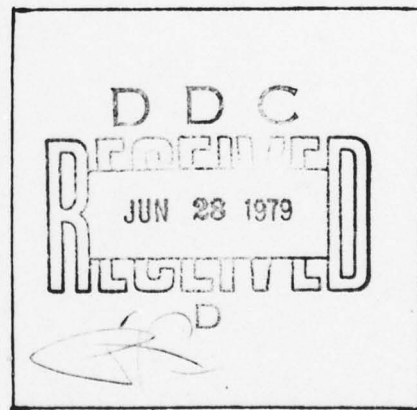
DOCUMENT IDENTIFICATION Uhm, Davidson, Chu

<p>DISTRIBUTION STATEMENT A</p> <p>Approved for public release; Distribution Unlimited</p>

DISTRIBUTION STATEMENT

Accession For	
NTIS GRA&I	<input checked="" type="checkbox"/>
DDC TAB	<input type="checkbox"/>
Unannounced	<input type="checkbox"/>
Justification	<input type="checkbox"/>
By _____	
Distribution/ _____	
Availability Codes	
Dist.	Avail and/or special
A	

DISTRIBUTION STAMP



DATE ACCESSIONED

79 06 27 302

DATE RECEIVED IN DDC

PHOTOGRAPH THIS SHEET

I. INTRODUCTION

One of the most basic instabilities that characterizes a hollow electron beam¹ with slow rotational equilibrium is the electron cyclotron maser instability.²⁻¹⁰ In recent experiments,^{4,5} the cyclotron maser instability has been investigated for magnetic harmonic number $s \geq 2$, with particular emphasis on the implications for intense microwave generation. Previous theoretical analyses of this instability have been carried out for a non-self-consistent equilibrium slab configuration.^{6,8} Strictly speaking, a more accurate theoretical model of microwave generation by the cyclotron maser instability, including a determination of the optimum value of the beam radius R_0 , requires a linear stability analysis for perturbations about a self-consistent, cylindrical, Vlasov equilibrium.

This paper develops a self-consistent theory¹⁰ of the cyclotron maser instability for azimuthally symmetric perturbations with magnetic harmonic number $s \geq 1$. The present work extends the previous self-consistent theory¹⁰ of the cyclotron maser instability, developed by the authors for $s=1$, to higher values of magnetic harmonic number ($s \geq 2$). The analysis is carried out within the framework of the Vlasov-Maxwell equations for an infinitely long electron beam propagating parallel to a uniform magnetic field $B_0 \hat{e}_z$ with axial velocity $v_b \hat{e}_z$. We assume that the beam is very tenuous, so that the perturbed field can be approximated by the vacuum waveguide fields ($v/\gamma_0 \ll 1$, where v is Budker's parameter). Equilibrium and stability properties are calculated for the specific choice of equilibrium electron distribution function in which all electrons have the same value of canonical angular momentum (P_0) and the same value of energy ($\gamma_0 mc^2$) in a frame

79 00 37 802

of reference moving with axial velocity $\beta_b c$ [Eq. (5)]. Equilibrium properties are examined in Sec. II. An important feature of the analysis is that the equilibrium distribution function in Eq. (5) corresponds to a hollow density profile with sharp radial boundaries [Eq. (13)].

The formal stability analysis for azimuthally symmetric electromagnetic perturbations ($\partial/\partial\theta=0$) is carried out in Sec. III. Making use of the fact that the electron trajectories are circular, the perturbed distribution function is calculated for arbitrary magnetic harmonic numbers [Eqs. (38) and (39)]. Equations (38) and (39), when combined with Eqs. (16), (22), (23), and (24), constitute one of the main results of this paper and can be used to investigate stability properties for a broad range of system parameters. In this regard, we emphasize that Eqs. (38) and (39) are derived with no a priori assumption that the electron motion in the beam frame is much smaller than the speed of light in vacuo, i.e., that $\beta_0^2 = (1 - 1/\gamma_0^2) \ll 1$.

In Sec. IV, a detailed analytic investigation of the cyclotron maser instability is carried out for the TE and TM waveguide modes, assuming $\beta_0^2 \ll 1$. Introducing the normalized Doppler shifted eigenfrequency [Eq. (49)]

$$x_s = [\gamma_b (\omega - kV_b) - s\omega_c] / \omega_c ,$$

the dispersion relation can be expressed as [Eqs. (48) and (51)]

$$x_s^3 - Q_{sn}^E x_s + \beta_0^2 s Q_{sn}^E / (2s+1) = 0, \text{ TE mode,}$$

$$x_1^3 - Q_{1n}^M x_1 + \beta_0^2 Q_{1n}^M / 5 = 0, \text{ TM mode,}$$

where $\gamma_b = 1/(1 - \beta_b^2)^{1/2}$, $\omega_c = eB_0/\gamma_0 mc$ is the electron cyclotron frequency in a frame of reference moving with axial velocity $\beta_b c \hat{e}_z$, k is the axial

wavenumber, ω is the complex eigenfrequency, Q_{sn}^E (Q_{1n}^M) is the coupling coefficient for the TE (TM) mode [Eqs. (50) and (52)], and $s=1, 2, 3\dots$ denotes the magnetic harmonic number. Evidently, for given s which satisfies $\alpha_{s1} < \alpha_{0n}$ for the TE mode and $\alpha_{s1} < \beta_{0n}$ for the TM mode, the maximum growth rate occurs at a value of R_0/R_c given by [Eq. (53)]

$$R_0/R_c = \begin{cases} \alpha_{s1}/\alpha_{0n}, & \text{TE mode,} \\ \alpha_{s1}/\beta_{0n}, & \text{TM mode,} \end{cases}$$

where α_{s1} is the first zero of $J'_s(y)=0$, and α_{0n} and β_{0n} are the n th zeroes of $J_1(y)=0$ and $J_0(y)=0$, respectively.

A detailed numerical analysis of the dispersion relations in Eqs. (48) and (51) is presented in Sec. V, where stability properties are investigated for a broad range of system parameters. It is found that the growth rate of perturbations with $s \geq 2$ increases rapidly when the value of β_0 is increased. We therefore conclude, for moderate or high values of β_0 , that magnetic harmonic perturbations with $s \geq 2$ are also important unstable modes for intense microwave generation by the cyclotron maser instability.

Finally, we note that Eqs. (53) and (30) can be combined to determine the conditions for maximum growth rate and hence optimum conditions for intense microwave generation by the cyclotron maser instability. In particular, the microwave frequency $\omega = s\omega_c \gamma_b$ produced by the electron beam can be tuned by the matching condition $R_c = \alpha_{0n} c / s\omega_c$ in Eq. (30). Moreover, selecting $R_0/R_c = \alpha_{s1}/\alpha_{0n}$ maximizes the growth rate of the TE mode perturbation with magnetic harmonic number s (Sec. IV and V).

II. EQUILIBRIUM PROPERTIES AND BASIC ASSUMPTIONS

As illustrated in Fig. 1, the equilibrium configuration consists of a slowly rotating hollow electron beam that propagates parallel to a uniform applied magnetic field $B_0 \hat{e}_z$ with mean axial velocity $\beta_b c \hat{e}_z$. The mean radius of the electron beam is denoted by R_0 and a grounded cylindrical conducting wall is located at radius $r=R_c$. The applied magnetic field provides radial confinement of the electrons, and the radial thickness of the electron beam is denoted by $2a$. As shown in Fig. 1, we introduce a cylindrical polar coordinate system (r, θ, z) with the z -axis coinciding with the axis of symmetry; r is the radial distance from the z -axis, and θ is the polar angle in a plane perpendicular to the z -axis.

The following are the main assumptions pertaining to the present analysis:

(a) Equilibrium properties are independent of z ($\partial/\partial z=0$) and azimuthally symmetric ($\partial/\partial \theta=0$) about the z -axis.

(b) The mean canonical angular momentum of the electrons is negative, which corresponds to a slow rotational equilibrium.^{1,10}

(c) It is further assumed that

$$v/\gamma_0 \ll 1 \quad (1)$$

where $v=N_e e^2/mc^2$ is Budker's parameter,

$$N_e = 2\pi \int_0^{R_c} dr r n_e^0(r) \quad (2)$$

is the number of electrons per unit axial length, $n_e^0(r)$ is the equilibrium electron density, c is the speed of light in vacuo, $-e$ and m are the charge and rest mass, respectively, of an electron,

and $\gamma_0 mc^2$ is the electron energy in a frame of reference moving with the mean axial velocity $V_b \hat{e}_z$ of the electron beam. The inequality in Eq. (1) indicates that the beam is very tenuous, so that the perturbed fields can be approximated by the vacuum waveguide fields.¹⁰ Consistent with the low-density assumption in Eq. (1), we also neglect the influence of the small equilibrium self-electric and self-magnetic fields that are produced by the lack of equilibrium charge and current neutralization.

For azimuthally symmetric equilibria with $\partial/\partial\theta=0=\partial/\partial z$, there are three single-particle constants of the motion. These are the total energy H ,

$$H = \gamma mc^2 = (m^2 c^4 + c^2 p^2)^{1/2}, \quad (3)$$

the canonical angular momentum P_θ ,

$$P_\theta = r[p_\theta - (e/2c)rB_0] \quad (4)$$

and the axial canonical momentum $P_z = p_z$. In Eqs. (3) and (4), lower case p denotes mechanical momentum and the equilibrium self-fields have been neglected in comparison with the external magnetic field $B_0 \hat{e}_z$ [see Eq. (1)]. Any distribution function that is a function only of the single-particle constants of the motion satisfies the steady-state Vlasov equation ($\partial/\partial t=0$). For present purposes, we assume an equilibrium distribution function of the form,^{1,10}

$$f_e^0(H, P_\theta, P_z) = \frac{n_0 R_0}{2\pi m \gamma_b \gamma_0} \delta(U) \delta(P_\theta - P_0), \quad (5)$$

where $n_0 = \text{const.}$ is the electron density at $r=R_0$, $P_0 = -(e/2c)(R_0^2 - a^2)B_0 = \text{const}$ is the canonical angular momentum of the electrons,

$$U = H - \beta_b c p_z - \gamma_0 mc^2 / \gamma_b \quad (6)$$

is an effective energy variable, $\beta_b = \text{const.}$ is defined by $\beta_b = v_b/c = (\gamma_b^2 - 1)^{1/2}/\gamma_b$, and γ_0 and γ_b are constants. It is straightforward to show that the axial velocity profile associated with Eq. (5) is uniform over the beam cross section.¹⁰

Several pertinent equilibrium properties can be deduced for the class of electron beam equilibria described by Eq. (5). For this purpose, it is useful to transform the energy variable U defined in Eq. (6) from momentum variables (p_r, p_θ, p_z) appropriate to the laboratory frame to momentum variables (p'_r, p'_θ, p'_z) appropriate to a frame of reference moving with velocity $\beta_b c \hat{e}_z$, where \hat{e}_z is a unit vector in the z -direction. The relevant transformation^{1,10} is given by

$$p_r = p'_r, \quad p_\theta = p'_\theta, \quad p_z = \gamma_b (p'_z + \gamma' m \beta_b c), \quad \gamma = \gamma_b (\gamma' + \beta_b p'_z / mc), \quad (7)$$

and

$$U = \frac{1}{\gamma_b} (\gamma' - \gamma_0) mc^2, \quad (8)$$

where $\gamma = (1 + p^2/m^2 c^2)^{1/2}$ and $\gamma' = (1 + p'^2/m^2 c^2)^{1/2}$. After some straightforward algebra, we find

$$f_e^0(H, p_\theta, p_z) d^3 p = \frac{n_0 R_0 (\gamma' + \beta_b p'_z / mc)}{2\pi m \gamma_0 \gamma'} \delta(\gamma' mc^2 - \gamma_0 mc^2) \delta(p'_\theta - p_\theta) d^3 p', \quad (9)$$

where $d^3 p = dp_r dp_\theta dp_z$ and $d^3 p' = dp'_r dp'_\theta dp'_z$. It is evident from Eq. (9) that $\gamma_0 mc^2$ can be identified with the total electron energy in a frame of reference moving with axial velocity $\beta_b c$.

The energy variable $\gamma' mc^2$ in Eq. (9) can be expressed as

$$\gamma' mc^2 = c(m^2 c^2 + m^2 \hat{\omega}_g^2 + p_\perp'^2)^{1/2} \quad (10)$$

where use has been made of $p_\theta = p'_\theta$, g is defined by

$$g(r) = \frac{R_0}{r} [\rho + (\rho^2 + a^2)/2R_0] , \quad (11)$$

$\hat{\omega}_c = eB_0/mc$ is the nonrelativistic electron cyclotron frequency, and $p_i'^2 = p_r'^2 + p_z'^2$. In Eq. (11) ρ is defined by

$$\rho = r - R_0 . \quad (12)$$

Substituting Eq. (11) into Eq. (9), and representing

$$\int d^3 p' = \int_{-\infty}^{\infty} dp'_\theta \int_0^{2\pi} d\alpha \int_0^{\infty} dp'_i p'_i ,$$

it is straightforward to show that the electron density can be expressed as

$$n_e^0(r) = \int d^3 p f_e^0(H, P_\theta, P_z) = n_0 \frac{R_0}{r} \Phi(a^2 - \rho^2) , \quad (13)$$

where

$$a = (\gamma_0^2 - 1)^{1/2} c / \hat{\omega}_c \quad (14)$$

is the half-thickness of the beam, and $\Phi(x)$ is the Heaviside step function defined by

$$\Phi = \begin{cases} 0 , & x < 0 , \\ 1 , & x > 0 . \end{cases}$$

The self-consistent electron density profile is illustrated in Fig. 2. Evidently, the electron beam equilibrium described by Eq. (5) has sharp radial boundaries. Additional equilibrium properties associated with the distribution function in Eq. (5) are discussed in Refs. 1 and 10.

III. LINEARIZED VLASOV-MAXWELL EQUATIONS FOR TENUOUS BEAM

In this section, we make use of the linearized Vlasov-Maxwell equations to investigate stability properties for azimuthally symmetric perturbations ($\partial/\partial\theta=0$) about a tenuous, hollow-beam equilibrium described by Eq. (5). We adopt a normal-mode approach in which all perturbations are assumed to vary with time and z according to

$$\delta\psi(\mathbf{x}, t) = \hat{\psi}(\mathbf{r}) \exp\{i(kz - \omega t)\},$$

where $\text{Im}\omega > 0$. Here ω is the complex eigenfrequency and k is the axial wavenumber. The Maxwell equations for the perturbed electric and magnetic field amplitudes can be expressed as

$$\nabla \times \hat{\mathbf{E}}(\mathbf{x}) = i \frac{\omega}{c} \hat{\mathbf{B}}(\mathbf{x}), \quad (15)$$

$$\nabla \times \hat{\mathbf{B}}(\mathbf{x}) = \frac{4\pi}{c} \hat{\mathbf{J}}(\mathbf{x}) - i \frac{\omega}{c} \hat{\mathbf{E}}(\mathbf{x}),$$

where

$$\hat{\mathbf{J}}(\mathbf{x}) = -e \int d^3 p \mathbf{v} \hat{f}_e(\mathbf{x}, \mathbf{p}) \quad (16)$$

is the perturbed current density. In Eq. (16),

$$\hat{f}_e(\mathbf{x}, \mathbf{p}) = e \int_{-\infty}^0 d\tau \exp\{-i\omega\tau\} \left\{ \hat{\mathbf{E}}(\mathbf{x}') + \frac{\mathbf{v}' \times \hat{\mathbf{B}}(\mathbf{x}')}{c} \right\} \cdot \frac{\partial}{\partial \mathbf{p}'} f_e^0 \quad (17)$$

is the perturbed distribution function, $\tau = t' - t$, and the particle trajectories $\mathbf{x}'(t')$ and $\mathbf{p}'(t')$ satisfy $d\mathbf{x}'/dt' = \mathbf{v}'$ and $d\mathbf{p}'/dt' = -e\mathbf{v}' \times \mathbf{B}_{0z} \hat{\mathbf{e}}_z / c$, with "initial" conditions $\mathbf{x}'(t'=t) = \mathbf{x}$ and $\mathbf{v}'(t'=t) = \mathbf{v}$.

In the tenuous beam limit consistent with Eq. (1), the perturbed fields can be approximated by the vacuum waveguide fields.¹⁰

In this context, the present stability analysis utilizes the vacuum transverse electric (TE) and transverse magnetic (TM) waveguide modes

as a convenient basis to represent a general electromagnetic field perturbation within a cylindrical waveguide. Making use of Eq. (15) and neglecting the perturbed current density, the vacuum waveguide modes can be expressed as

$$\hat{B}_z(r) = J_0(\alpha_{0n} r/R_c) = -i(c/\omega r) [\partial(r\hat{E}_\theta)/\partial r] = i[\partial(r\hat{B}_r)/\partial r]/kr, \quad (18)$$

for the TE mode and

$$\hat{E}_z(r) = J_0(\beta_{0n} r/R_c) = i(c/\omega r) [\partial(r\hat{B}_\theta)/\partial r] = i[\partial(r\hat{E}_r)/\partial r]/kr, \quad (19)$$

for the TM mode. In Eqs. (18) and (19), $J_\ell(x)$ is the Bessel function of first kind of order ℓ , and α_{0n} and β_{0n} are the n th roots of $J_1(\alpha_{0n})=0$ and $J_0(\beta_{0n})=0$, respectively. Moreover, without loss of generality, the normalization amplitudes for $\hat{B}_z(r=0)$ and $\hat{E}_z(r=0)$ have been set equal to unity in Eqs. (18) and (19). After a simple algebraic manipulation of Eqs. (15), (18), and (19), it is straightforward to show that

$$\left(\frac{\omega^2}{c^2} - k^2 - \frac{\alpha_{0n}^2}{R_c^2}\right) J_1(\alpha_{0n} r/R_c) = -4\pi(\alpha_{0n}/R_c) \hat{J}_\theta(r), \quad (20)$$

for the TE mode and

$$\left(\frac{\omega^2}{c^2} - k^2 - \frac{\beta_{0n}^2}{R_c^2}\right) J_0(\beta_{0n} r/R_c) = 4\pi ik[\hat{\rho}_e(r) - (\omega/kc^2)\hat{J}_z(r)] \quad (21)$$

for the TM mode. In Eq. (21), the perturbed charge density $\hat{\rho}_e(r)$ is defined by

$$\hat{\rho}_e(r) = -e \int d^3p \hat{f}_e(r, p). \quad (22)$$

Multiplying Eqs. (20) and (21) by $rJ_1(\alpha_{0n} r/R_c)$ and $rJ_0(\beta_{0n} r/R_c)$, respectively, and integrating from $r=0$ to $r=R_c$, we obtain

$$\left(\frac{\omega^2}{c^2} - k^2 - \frac{\alpha_{0n}^2}{R_c^2}\right) = - \frac{8\pi\alpha_{0n}/R_c c}{[R_c J_2(\alpha_{0n})]^2} \int_0^{R_c} dr r J_1(\alpha_{0n} r/R_c) \hat{J}_\theta(r) \quad (23)$$

for the TE mode and

$$\left(\frac{\omega^2}{c^2} - k^2 - \frac{\beta_{0n}^2}{R_c^2}\right) = \frac{8\pi i k}{[R_c J_1(\beta_{0n})]^2} \int_0^{R_c} dr r J_0(\beta_{0n} r/R_c) \left[\hat{\rho}_e(r) - \frac{\omega}{kc^2} \hat{J}_z(r) \right] \quad (24)$$

for the TM mode. For present purposes it is also assumed that

$$|\Omega_s| = |\omega - kV_b - s\omega_c/\gamma_b| \ll \omega_c/\gamma_b \quad (25)$$

where $\Omega_s = \omega - kV_b - s\omega_c/\gamma_b$ is the Doppler shifted frequency, $\omega_c = eB_0/\gamma_0 mc$ is the electron cyclotron frequency in a frame of reference moving with axial velocity V_b , and $s=1,2,3\dots$ denotes the magnetic harmonic number.

To lowest order, the eigenfrequency ω and axial wavenumber k are obtained from the simultaneous solution of the vacuum waveguide mode dispersion relation,

$$\frac{\omega^2}{c^2} - k^2 = \begin{cases} \alpha_{0n}^2/R_c^2 & , \text{ TE mode ,} \\ \beta_{0n}^2/R_c^2 & , \text{ TM mode ,} \end{cases} \quad (26)$$

and the condition for cyclotron resonance

$$\omega \approx kV_b + s\omega_c/\gamma_b . \quad (27)$$

Moreover, to maximize the growth rate and efficiency of microwave generating it is required that the group velocity of the vacuum waveguide mode in Eq. (26) be approximately equal to the beam velocity,¹⁰ i.e.,

$$v_g = \frac{d\omega}{dk} = \frac{kc^2}{\omega} \approx v_b . \quad (28)$$

Solving Eqs. (27) and (28) for the characteristic frequency and axial wave-number $(\omega, k) = (\omega_0, k_0)$, we find (Fig. 3)

$$\begin{aligned}\omega_0 &= s\omega_c \gamma_b, \\ k_0 &= s\omega_c \gamma_b \beta_b / c,\end{aligned}\tag{29}$$

where $\gamma_b = (1 - \beta_b^2)^{-1/2}$. For maximum growth, it is also required that (ω_0, k_0) solve Eq. (26) in leading order. Therefore, for maximum growth, we find that R_c should satisfy

$$R_c \approx \begin{cases} \alpha_{0n} c / s\omega_c, & \text{TE mode,} \\ \beta_{0n} c / s\omega_c, & \text{TM mode,} \end{cases}\tag{30}$$

for intense microwave generation at frequency $\omega \approx s\omega_c \gamma_b$. Because of the discrete nature of α_{0n} , β_{0n} , and s , we also conclude that the stability analysis can be carried out separately for the TE and TM modes.

The perturbed distribution function is calculated for the case of a self-consistent Vlasov equilibrium in which all electrons have the same canonical angular momentum and the same total energy in a frame of reference moving with axial velocity $V_b \hat{e}_z$ [Eqs. (5) and (9)]. To simplify the right-hand side of Eq. (17), we make use of Eqs. (4) and (6), and the identities $\partial U / \partial p_z = v_z - V_b \hat{e}_z$ and $\partial P_\theta / \partial p_\theta = r \hat{e}_\theta$, where \hat{e}_θ is a unit vector in the θ -direction. The TE mode portion of the perturbed distribution function can then be expressed as¹⁰

$$\begin{aligned}\hat{f}_e^E(r, p) &= \int_{-\infty}^0 d\tau \exp\{i[(kp_z / \gamma m) - \omega]\tau\} \left\{ \left(1 - \frac{kv_b}{\omega}\right) \hat{E}_\theta(r') v'_\theta \frac{\partial f_e^0}{\partial U} \right. \\ &\quad \left. + r' \left[\left(1 - \frac{kp_z}{\gamma m \omega}\right) \hat{E}_\theta(r') - \frac{v'_r}{c} B_z(r') \right] \frac{\partial f_e^0}{\partial P_\theta} \right\},\end{aligned}\tag{31}$$

which is required to calculate the perturbed azimuthal current density $\hat{J}_\theta(r)$ in Eq. (23). Similarly, the TM portion of the perturbed

distribution function is given by¹⁰

$$\hat{f}_e^M(r, p) = e \frac{\partial f_e^0}{\partial U} \int_{-\infty}^0 d\tau \exp\{i[(kp_z/\gamma m) - \omega]\tau\} \{[\hat{E}_r(r') - \beta_b \hat{B}_\theta(r')] v_r' + \hat{E}_z(r') [(p_z/\gamma m) - v_b]\} , \quad (32)$$

which is required to calculate the perturbed charge and axial current densities in Eq. (24). In obtaining Eqs. (31) and (32), use has been made of the axial orbit

$$z' = z + (p_z/\gamma m)(t' - t) .$$

The transverse (radial and azimuthal) motion of a typical electron is illustrated in Fig. 4. (The dotted circle is the electron orbit in a plane perpendicular to the z -axis.) The radial distance of the electron from the z -axis at times $t'=t$ and $t'=t'$ are denoted by r and r' , respectively. The point C is the gyrocenter of the electron trajectory. The angular coordinates ϕ and ϕ' are the perpendicular velocity-space polar angles at times $t'=t$ and $t'=t'$, and are related by

$$\phi' = \phi + (\hat{\omega}_c/\gamma)(t' - t) .$$

The transverse velocities at times $t'=t$ and $t'=t'$ are denoted, respectively, by v_{T} and v_{T}' , and the corresponding speeds are defined by $v_T = (v_r^2 + v_\theta^2)^{1/2}$ and $v_T' = (v_r'^2 + v_\theta'^2)^{1/2}$.

To simplify the present analysis, we also assume that

$$v/\gamma_0 \ll (\beta_0 \omega_c R_c/c)^2 , \quad (33)$$

where $\beta_0 = (1 - 1/\gamma_0^2)^{1/2}$. Equation (33) is easily satisfied in parameter regimes of experimental interest.²⁻⁵ Within the context of Eq. (33), it is valid for $s \leq 3$ to neglect the terms proportional to $\partial f_e^0/\partial p_\theta$ in

Eq. (31), since the corrections associated with these terms are of order $(v/\gamma_0)(c/\beta_0\omega_c R_c)^2$ ($\ll 1$) or smaller. Substituting Eq. (18) into Eq. (31), we find that the perturbed TE mode distribution function can be approximated by

$$\hat{f}_e^E(r, \rho) = \frac{ieR_c}{\alpha_{0n}c} (\omega - kv_b) \frac{p_T}{\gamma m} \frac{\partial f_e^0}{\partial U} \int_{-\infty}^0 d\tau \exp\{i[(kp_z/\gamma m) - \omega]\tau\} \\ \times \sin(\phi' - \theta') J_1(\alpha_{0n} r'/R_c), \quad (34)$$

where $p_T = \gamma m v_T = (p_r^2 + p_\theta^2)^{1/2}$, and use has been made of $v'_\theta = v_T \sin(\phi' - \theta')$. Making use of Eq. (28) and substituting Eq. (19) into Eq. (32), we obtain

$$\hat{f}_e^M(r, \rho) = e[(p_z/\gamma m) - v_b] \frac{\partial f_e^0}{\partial U} \int_{-\infty}^0 d\tau \exp\{i[(kp_z/\gamma m) - \omega]\tau\} J_0(\alpha_{0n} r'/R_c) \quad (35)$$

for the perturbed TM mode distribution function.

The Bessel function summation theorem for the triangle OAB in Fig. 4 can be expressed as¹¹

$$\exp\{i\ell(\theta' - \theta)\} J_\ell(\alpha_{0n} r'/R_c) = \sum_{s'=-\infty}^{\infty} J_{\ell+s'}(\alpha_{0n} r'/R_c) J_{s'}(\alpha_{0n} \lambda/R_c) \\ \times \exp\{is'(\pi + \theta - \phi - \hat{\omega}_c \tau/2\gamma)\}. \quad (36)$$

Similarly, for the triangle ABC, we can represent

$$\exp\{i \frac{s'}{2} (\pi - \hat{\omega}_c \tau/\gamma)\} J_{s'}(\alpha_{0n} \lambda/R_c) \\ = \sum_{s=-\infty}^{\infty} J_{s+s'}(\frac{\alpha_{0n} p_T}{m \hat{\omega}_c R_c}) J_s(\frac{\alpha_{0n} p_T}{m \hat{\omega}_c R_c}) \exp\{is \hat{\omega}_c \tau/\gamma\}, \quad (37)$$

where $s=1, 2, 3, \dots$ denotes the magnetic harmonic number. Making use of Eqs. (28), (36), and (37), and carrying out the time integration

in Eq. (34), it is straightforward to show, for a given harmonic component s , that the perturbed TE mode distribution function can be approximated by

$$\hat{f}_{es}^E(r, \rho) = \frac{eR_c}{\alpha_{0n}c} \frac{(\omega - kV_b)p_T}{2\gamma_b^m} \frac{\partial f_e^0}{\partial U} \frac{J_{s-1}\left(\frac{\alpha_{0n}P_T}{m\hat{\omega}_c R_c}\right) - J_{s+1}\left(\frac{\alpha_{0n}P_T}{m\hat{\omega}_c R_c}\right)}{\gamma'(\omega - kV_b) - s\hat{\omega}_c/\gamma_b} \quad (38)$$

$$\times \sum_{s'} (i)^{s'} J_{s'}(\alpha_{0n}r/R_c) J_{s+s'}\left(\frac{\alpha_{0n}P_T}{m\hat{\omega}_c R_c}\right) \exp\{is'(\theta - \phi)\},$$

where use has been made of the Lorentz transformation in Eq. (7).

In obtaining Eq. (38), we have neglected the mode coupling between different values of s , which is consistent with Eq. (25). In a similar manner, the perturbed TM mode distribution function for harmonic component s can be approximated by

$$\hat{f}_{es}^M(r, \rho) = \frac{ie}{\gamma_b^2} \frac{p'_z(\partial f_e^0/\partial U)}{\gamma'(\omega - kV_b) - s\hat{\omega}_c/\gamma_b} J_s\left(\frac{\beta_{0n}P_T}{m\hat{\omega}_c R_c}\right) \quad (39)$$

$$\times \sum_{s'} (i)^{s'} J_{s'}(\beta_{0n}r/R_c) J_{s+s'}\left(\frac{\beta_{0n}P_T}{m\hat{\omega}_c R_c}\right) \exp\{is'(\theta - \phi)\}.$$

Equations (38) and (39), when combined with Eqs. (16), (22), (23), and (24), constitute one of the main results of this paper and can be used to investigate stability properties for a broad range of system parameters. In this regard, we emphasize that Eqs. (38) and (39) have been derived with no a priori assumption that $\beta_0^2 \equiv (1 - 1/\gamma_0^2) \ll 1$ or that $a \ll R_0$. However, in the limiting case where $\beta_0^2 \ll 1$, Eqs. (38) and (39) can be simplified considerably (Sec. IV).

IV. CYCLOTRON MASER INSTABILITY FOR $\beta_0^2 \ll 1$

In this section, simplified expressions are obtained for the perturbed distribution function in Eqs. (38) and (39), and the results are used to derive the dispersion relation for several different values of magnetic harmonic numbers. The present analysis assumes that the electron motion in a frame of reference moving with axial velocity $\beta_b c$ is much smaller than speed of light in vacuo, i.e., that

$$\beta_0^2 = 1 - 1/\gamma_0^2 \ll 1. \quad (40)$$

Equation (40) can be used to truncate the summations over s' in Eqs. (38) and (39), keeping only leading terms of order β_0^2 . Defining Q_{sn}^E and Q_{sn}^M to be the coupling coefficients between the vacuum TE and TM waveguide modes and the cyclotron resonance mode $\omega = kV_b + s\omega_c/\gamma_b$, it is found that $|Q_{sn}^M/Q_{sn}^E| \leq \beta_0^2/4$ [see Eqs. (50) and (52)]. In this context ($\beta_0^2 \ll 1$), the instability growth rate is largest for the TE mode.

The perturbed distribution function in Eqs. (38) and (39) can be further simplified by making use of the symmetry properties of the equilibrium distribution function $f_e^0(U, P_\theta)$. Since the variable U is an even function of p_r [Eq. (8)], it follows from Eqs. (16) and (22) that any term in Eqs. (38) and (39) that is an odd function of p_r will give zero when the integration over p_r is carried out. Therefore, when evaluating $\hat{f}_{es}(r, p)$, we simply omit terms proportional to odd functions of p_r . To evaluate the momentum integral in Eqs. (16) and (22), use is made of Eq. (10). After some straightforward algebra, we find

$$\begin{aligned}
\int d^3 p \frac{1}{\gamma} \frac{\partial f_e^0 / \partial U}{\gamma' (\omega - kV_b) - s\hat{\omega}_c / \gamma_b} &= - \frac{n_0 R_0}{\gamma_0 m \hat{\omega}_c^2 r} \left\{ \frac{1}{a \Omega_s} \left[\left(1 + \frac{a}{R_0}\right) \delta(\rho - a) \right. \right. \\
&\quad \left. \left. + \left(1 - \frac{a}{R_0}\right) \delta(\rho + a) \right] - \frac{\beta_0^2 (\omega - kV_b)}{a^2 \Omega_s^2} \Theta(a^2 - \rho^2) \right\}, \\
\int d^3 p \frac{p_r^2}{\gamma} \frac{\partial f_e^0 / \partial U}{\gamma' (\omega - kV_b) - s\hat{\omega}_c / \gamma_b} &= \frac{1}{\gamma_b} \int d^3 p' \frac{p_z'^2}{\gamma'} \frac{\partial f_e^0 / \partial U}{\gamma' (\omega - kV_b) - s\hat{\omega}_c / \gamma_b} \\
&= - \frac{n_0 R_0 m}{\gamma_0 r} \left[\frac{1}{\Omega_s} - \frac{\beta_0^2 (a^2 - g^2) (\omega - kV_b)}{2a^2 \Omega_s^2} \right] \Theta(a^2 - \rho^2), \\
\int d^3 p \frac{p_r^4}{\gamma} \frac{\partial f_e^0 / \partial U}{\gamma' (\omega - kV_b) - s\hat{\omega}_c / \gamma_b} &= \frac{3}{\gamma_b} \int d^3 p' \frac{(p_r' p_z')^2}{\gamma'} \frac{\partial f_e^0 / \partial U}{\gamma' (\omega - kV_b) - s\hat{\omega}_c / \gamma_b} \\
&= - \frac{3n_0 R_0 m^3 \hat{\omega}_c^2}{2\gamma_0 r} (a^2 - g^2) \left[\frac{1}{\Omega_s} - \frac{\beta_0^2 (\omega - kV_b) (1 - g^2/a^2)}{4\Omega_s^2} \right] \Theta(a^2 - \rho^2), \tag{41}
\end{aligned}$$

where the Doppler shifted frequency Ω_s is defined in Eq. (25), and $g(r)$ is defined in Eq. (11).

We first investigate stability properties for the TE mode perturbation with fundamental magnetic harmonic number ($s=1$). From Eq. (38), the perturbed distribution function is approximated by

$$\hat{f}_{e1}^E(r, \rho) = - \frac{eR_c}{\alpha_{0n} c} \frac{\omega - kV_b}{2\gamma_b m} J_1(\alpha_{0n} r/R_c) \frac{p_\theta \partial f_e^0 / \partial U}{\gamma' (\omega - kV_b) - \hat{\omega}_c / \gamma_b}, \tag{42}$$

where $p_\theta = p_T \sin(\phi - \theta) = m\hat{\omega}_c g$. The perturbed azimuthal current density is evaluated by substituting Eq. (42) into Eq. (16) and making use of Eq. (41). After some algebra, we obtain

$$\begin{aligned}
J_{\theta 1}^E(r) &= - \frac{n_0 e^2 R_0 R_c (\omega - kV_b)}{2\gamma_0 \gamma_b m \alpha_{0n} c r} J_1(\alpha_{0n} r/R_c) g^2 \left\{ \frac{1}{a \Omega_1} \left[\left(1 + \frac{a}{R_0}\right) \delta(\rho - a) \right. \right. \\
&\quad \left. \left. + \left(1 - \frac{a}{R_0}\right) \delta(\rho + a) \right] - \frac{\beta_0^2 (\omega - kV_b)}{a^2 \Omega_1^2} \Theta(a^2 - \rho^2) \right\}. \tag{43}
\end{aligned}$$

The radial integration on the right-hand side of Eq. (23) can be carried out by Taylor expanding the integrand about $r=R_0$, and keeping leading terms of order $\rho^2=(r-R_0)^2$. The Taylor expansion of the Bessel functions provides a good approximation when the functions are slowly varying over the minor cross section of the beam. The number of electrons per unit axial length of the beam (N_e) can be determined by substituting Eq. (13) into Eq. (2), which gives $N_e=4\pi n_0 R_0$. Eliminating n_0 in favor of N_e and carrying out some straightforward algebraic manipulation, we obtain the $s=1$ TE mode dispersion relation

$$\frac{\omega^2}{c^2} - k^2 - \frac{\alpha_{0n}^2}{R_c^2} = \frac{2v}{\gamma_0 \gamma_b} \left(\frac{J_1(\alpha_{0n} R_0 / R_c)}{R_c J_2(\alpha_{0n})} \right)^2 \left(\frac{\omega - kV_b}{\omega - kV_b - \omega_c / \gamma_b} - \frac{\beta_0^2 (\omega - kV_b)^2}{3(\omega - kV_b - \omega_c / \gamma_b)^2} \right), \quad (44)$$

where use has been made of $v=N_e e^2 / mc^2$. The dispersion relation in Eq. (44) is identical to the result obtained previously by Uhm et al.¹⁰ for $s=1$.

In a similar manner, we have derived the dispersion relation for several values of magnetic harmonic number s . The following equations summarize the main analytic results obtained for $\beta_0^2 \equiv (1 - 1/\gamma_0^2) \ll 1$:

(a) The TM mode dispersion relation for $s=1$ is given by

$$\frac{\omega^2}{c^2} - k^2 - \frac{\beta_{0n}^2}{R_c^2} = \frac{2v\beta_0^2}{3\gamma_0 \gamma_b^3} \left(\frac{J_1(\beta_{0n} R_0 / R_c)}{R_c J_1(\beta_{0n})} \right)^2 \left(\frac{\omega}{\omega - kV_b - \omega_c / \gamma_b} - \frac{\beta_0^2 \omega (\omega - kV_b)}{5(\omega - kV_b - \omega_c / \gamma_b)^2} \right), \quad (45)$$

where use has been made of the recursion formula $J_0^2 - d(J_0 J_1) / dx = J_0 J_1 / x = J_1^2$.

(b) The TE mode dispersion relation for $s=2$ is given by

$$\frac{\omega^2}{c^2} - k^2 - \frac{\alpha_{0n}^2}{R_c^2} = \frac{8\nu\beta_0^2}{3\gamma_0\gamma_b} \left(\frac{J_2(\alpha_{0n}R_0/R_c)}{R_c J_2(\alpha_{0n})} \right)^2 \left(\frac{\omega - kV_b}{\omega - kV_b - 2\omega_c/\gamma_b} - \frac{\beta_0^2(\omega - kV_b)^2}{5(\omega - kV_b - 2\omega_c/\gamma_b)^2} \right), \quad (46)$$

where use has been made of

$$J_1^2 - d(J_1 J_2)/dx - J_1 J_2/x = J_2^2.$$

(c) The TE mode dispersion relation for $s=3$ is given by

$$\frac{\omega^2}{c^2} - k^2 - \frac{\alpha_{0n}^2}{R_c^2} = \frac{81\nu\beta_0^4}{20\gamma_0\gamma_b} \left(\frac{J_3(\alpha_{0n}R_0/R_c)}{R_c J_3(\alpha_{0n})} \right)^2 \left(\frac{\omega - kV_b}{\omega - kV_b - 3\omega_c/\gamma_b} - \frac{\beta_0^2(\omega - kV_b)^2}{7(\omega - kV_b - 3\omega_c/\gamma_b)^2} \right) \quad (47)$$

where use has been made of

$$J_3^2 = J_1^2 - 2d(J_1 J_2)/dx - 2J_1 J_2/x + d^2(J_1 J_3)/dx^2 + 3[d(J_1 J_3)/dx]/x.$$

Substituting Eq. (30) into Eqs. (44), (46), and (47), and making use of $\omega = kV_b + s\omega_c/\gamma_b$, we obtain the approximate TE mode dispersion relation

$$x_s^3 - Q_{sn}^E x_s + \beta_0^2 s Q_{sn}^E / (2s+1) = 0 \quad (48)$$

for $s=1,2,3$. In Eq. (48), the normalized Doppler-shifted eigenfrequency x_s is defined by

$$x_s = [\gamma_b(\omega - kV_b) - s\omega_c] / \omega_c, \quad (49)$$

and the coupling coefficients between the TE vacuum waveguide mode and the electron cyclotron resonance mode are defined by

$$\begin{aligned}
Q_{1n}^E(R_0/R_c) &= \nu [J_1(\alpha_{0n} R_0/R_c) / J_2(\alpha_{0n})]^2 / \gamma_0 \gamma_b \alpha_{0n}^2, \\
Q_{2n}^E(R_0/R_c) &= 16\nu \beta_0^2 [J_2(\alpha_{0n} R_0/R_c) / J_2(\alpha_{0n})]^2 / 3\gamma_0 \gamma_b \alpha_{0n}^2, \\
Q_{3n}^E(R_0/R_c) &= 9\nu (3\beta_0)^4 [J_3(\alpha_{0n} R_0/R_c) / J_2(\alpha_{0n})]^2 / 40\gamma_0 \gamma_b \alpha_{0n}^2.
\end{aligned} \tag{50}$$

Similarly, for the $s=1$ TM mode, we obtain

$$x_1^3 - Q_{1n}^M x_1 + \beta_0^2 Q_{1n}^M / 5 = 0, \tag{51}$$

where the coupling coefficient Q_{1n}^M is defined by

$$Q_{1n}^M(R_0/R_c) = \nu \beta_0^2 [J_1(\beta_{0n} R_0/R_c) / J_1(\beta_{0n})]^2 / 3\gamma_0 \gamma_b \beta_{0n}^2. \tag{52}$$

As mentioned at the beginning of this section, it is evident from Eqs. (50) and (52) that the TM mode coupling coefficient Q_{1n}^M is much less than the TE mode coupling coefficient Q_{1n}^E . Therefore, we conclude that the TE mode is the dominant unstable perturbation for $\beta_0^2 \ll 1$. However, when the transverse electron motion is relativistic ($\beta_0 \rightarrow 1$), the TM mode perturbation is equally important. A careful examination of Eqs. (50) and (52) shows that the coupling coefficient between the vacuum waveguide mode and the electron cyclotron resonance mode ($\omega = kV_b + s\omega_c / \gamma_b$) is a maximum whenever $J'_s(\alpha_{0n} R_0/R_c) = 0$ for the TE mode, and $J'_s(\beta_{0n} R_0/R_c) = 0$ for the TM mode. Here the prime (') denotes $dJ_s(x)/dx$. In this context, we find that the maximum growth rate for magnetic harmonic number s occurs for a value of R_0/R_c given by

$$R_0/R_c = \begin{cases} \alpha_{s1} / \alpha_{0n}, & \text{TE mode,} \\ \alpha_{s1} / \beta_{0n}, & \text{TM mode,} \end{cases} \tag{53}$$

where α_{s1} is the first root of $J'_s(\alpha_{s1}) = 0$. Equation (53) is valid only

when $\alpha_{s1} < \alpha_{0n}$ for the TE mode, and $\alpha_{s1} < \beta_{0n}$ for the TM mode. For $\alpha_{s1} > \alpha_{0n}$ (TE) or $\alpha_{s1} > \beta_{0n}$ (TM), the maximum growth rate occurs for $R_0/R_c \approx 1$. It should also be noted from Eq. (50) that perturbations with higher magnetic harmonic number become dominant when the transverse electron speed approaches c ($\beta_0 \rightarrow 1$). In the following section, we make use of Eqs. (48)-(52) to investigate detailed stability properties for a broad parameter range of experimental interest.

V. NUMERICAL ANALYSIS OF STABILITY PROPERTIES

The growth rate $\omega_i = \text{Im}\omega$ and real oscillation frequency $\omega_r = \text{Re}\omega$ have been calculated numerically from Eqs. (48) and (51) for a broad range of system parameters, R_0/R_c , n , s , β_0 , and β_b . Since the electron beam is hollow ($R_0 > a$) and is located inside a conducting waveguide of radius R_c ($R_0 < R_c - a$), the allowable range of R_0/R_c is restricted to

$$\begin{aligned} (s\beta_0/\alpha_{0n}) < (R_0/R_c) < 1 - s\beta_0/\alpha_{0n}, & \text{ TE mode,} \\ (s\beta_0/\beta_{0n}) < (R_0/R_c) < 1 - s\beta_0/\beta_{0n}, & \text{ TM mode,} \end{aligned} \quad (54)$$

where use has been made of Eq. (30). Therefore, in Figs. 5-7, the plots are presented only for values of R_0/R_c satisfying Eq. (54).

Shown in Fig. 5 are plots of (a) the normalized growth rate $\gamma_b \omega_i / \omega_c$ and (b) the normalized Doppler-shifted real frequency $\text{Re}(\gamma_b \Omega_1 / \omega_c) = [\gamma_b (\omega_r - kV_b) - \omega_c] / \omega_c$ versus R_0/R_c obtained from Eq. (48) (TE mode) for $s=1$, $v=0.001$, $\beta_0=0.4$, $\beta_b=0.286$, and several values of n . Several features are noteworthy from Fig. 5. First, the maximum growth rate decreases as the radial harmonic number n is increased. As evident from Eqs. (50) and (52), this feature represents a general tendency for both TE and TM perturbations, for all magnetic harmonic numbers s . Second, the number of zeroes of ω_i (where the growth rate vanishes) increases as n is increased. Moreover, the maximum value of the growth rate is also a decreasing function of R_0/R_c . Third, the plot of the Doppler-shifted real frequency versus R_0/R_c has the same general form as the plot of the growth rate versus R_0/R_c . However, the growth rate is about 1.5 times as large as the Doppler-shifted real frequency. This feature is a result of the fact that the contribu-

tion of the second term in Eq. (48) is negligible in comparison with the third term, for $\beta_0=0.4$. Fourth, the maximum growth rate occurs at a value of R_0/R_c corresponding to the maximum value of the perturbed azimuthal electric field [Eqs. (18) and (44)].

Shown in Fig. 6 are plots of the normalized growth rate $\gamma_b \omega_i / \omega_c$ versus R_0/R_c obtained from Eq. (51) (TM mode) for parameters identical to Fig. 5. Comparing Fig. 6 with Fig. 5(a), it is evident that the TE mode is more unstable than the TM mode. For example, for $n=1$, the maximum TE mode growth rate is $\omega_i \approx 0.0143 \omega_c / \gamma_b$, whereas the maximum TM mode growth rate is $\omega_i \approx 0.0055 \omega_c / \gamma_b$. In this context, we conclude that the TE mode is a more effective means for exciting microwave radiation, at least for modest values of β_0 . Since the plot of the Doppler-shifted real frequency has a similar form to the growth rate curve, it is not shown in Fig. 6 (see Fig. 5).

We now present an example that illustrates cyclotron maser stability properties for higher magnetic harmonic numbers ($s \geq 2$). Shown in Fig. 7 are plots of the normalized growth rate $\gamma_b \omega_i / \omega_c$ versus R_0/R_c obtained from Eq. (48) (TE mode) for (a) $s=2$ and (b) $s=3$, and parameters otherwise identical to Fig. 5. As evident from Fig. 7(a), the maximum growth rate for $s=2$ occurs for $R_0/R_c=0.78$ when $n=1$, for $R_0/R_c=0.44$ when $n=2$, and for $R_0/R_c=0.3$ when $n=3$. These values of R_0/R_c correspond to $R_0/R_c = \alpha_{21} / \alpha_{0n}$ [see Eq. (53)]. In Fig. 7(b) ($s=3$), the maximum growth rate for $n=2$ and $n=3$ also occur at $R_0/R_c=0.6$ and $R_0/R_c=0.41$, respectively. However, for $s=3$ and $n=1$, the growth rate assumes a maximum value for $R_0/R_c=0.69$, since $\alpha_{31} > \alpha_{01}$ [see Fig. 7(b)]. Evidently, the value of $R_0/R_c = \alpha_{s1} / \alpha_{0n}$ plays a very important role in determining optimum system parameters for intense microwave generation by the cyclotron maser instability.

Of considerable experimental interest is the stability behavior for specified n and several values of s . Typical results are shown in Fig. 8 where (a) the normalized maximum growth rate $(\gamma_b \omega_i / \omega_c)_m$ and (b) the normalized Doppler-shifted real frequency $\text{Re}(\gamma_b \Omega / \omega_c)$ are plotted versus β_0 for $n=2$ and $\nu=0.001$. In Fig. 8, we assume $\beta_b = \beta_0 / 1.4$, and the solid and dashed curves represent the TE and TM modes, respectively. The range of β_0 is limited to $0.1 \leq \beta_0 \leq 0.5$ since this stability analysis is valid only when $(\nu / \gamma_0) (c / R_c \omega_c)^2 \ll \beta_0^2 \ll 1$ [see Eqs. (33) and (40)]. In Fig. 8(b), the real frequency for the $s=1$ TE mode is related only for the range of β_0 corresponding to instability ($\omega_i > 0$). For the TE mode perturbation, maximum growth occurs at $R_0 / R_c = 0.26$ for $s=1$, at $R_0 / R_c = 0.44$ for $s=2$, and at $R_0 / R_c = 0.6$ for $s=3$, whereas the TM mode perturbation with $s=1$ has a maximum growth rate at $R_0 / R_c = 0.33$ [see also Figs. 5-7]. Note that the $s=1$ TE mode perturbation is stabilized by decreasing β_0 to $\beta_0 = 0.18$, which corresponds to $\beta_0 = (4Q_{12}^E / 3)^{1/4}$ (see Ref. 10). As shown in Fig. 8(a), the $s=1$ TE mode perturbation is the most unstable mode for small values of β_0 ($\beta_0 \leq 0.3$, say). However, the growth rate of perturbations with $s \geq 2$ increases rapidly when the value of β_0 is increased. As an example, for the $(s,n)=(3,2)$ TE mode, the maximum growth rate increases by a factor of six when β_0 is increased from 0.2 to 0.5. We therefore conclude that for moderate or high values of β_0 , perturbations with higher magnetic harmonic numbers ($s \geq 2$) are also important unstable modes for generating intense microwave radiation. We further note from Fig. 8 that the growth rate of the TM mode is comparable with that of the TE mode, when β_0 approaches unity.

Finally, we conclude this section by pointing out two important areas where the present analysis can be extended. First, as previously shown for $s=1$, it may also be possible to demonstrate analytically for higher magnetic harmonic numbers ($s \geq 2$) that the region of k -space corresponding to instability is very narrow-band with $kc \approx \omega \beta_D$. Second, the present stability analysis can be extended in a relatively straightforward manner to magnetic harmonic numbers $s \geq 4$, and also to higher values of β_0 ($\beta_0 \rightarrow 1$).

VI. CONCLUSIONS

In this paper, we have examined the excitation of electromagnetic waveguide modes by the cyclotron maser instability for magnetic harmonic number $s \geq 1$. The analysis was carried out for a hollow electron beam propagating parallel to a uniform magnetic field $B_0 \hat{e}_z$, assuming that the beam is very tenuous [Eq. (1)]. In Sec. II, equilibrium properties were calculated for the choice of electron distribution function in which all electrons have the same value of canonical angular momentum (P_0) and same value of energy ($\gamma_0 mc^2$) in a frame of reference moving with axial velocity $\beta_b c$ [Eq. (5)]. A formal stability analysis for azimuthally symmetric electromagnetic perturbation was carried out in Sec. III. Equations (38) and (39), when combined with Eqs. (16), (22), (23), and (24), constitute one of the main results of this paper and can be used to investigate stability properties for a broad range of system parameters. In Sec. IV, a detailed analytic investigation of the cyclotron maser instability was carried out for TE and TM waveguide modes, assuming $\beta_0^2 \equiv (1 - 1/\gamma_0^2) \ll 1$. The value of the geometric parameter R_0/R_c corresponding to maximum growth rate was determined, and a detailed numerical analysis of the dispersion relation was presented in Sec. V. One of the principal conclusions of this study is that for moderate or high value of β_0 ($\beta_0 > 0.3$, say) magnetic harmonic perturbations with $s \geq 2$ have growth rates comparable with the fundamental ($s=1$) mode. Moreover, the growth rate of perturbations with $s \geq 2$ increases rapidly when the value of β_0 is increased.

Finally, we emphasize that Eq. (53) together with Eq. (30), can be used to calculate conditions for maximum microwave generation by the cyclotron maser instability. By selecting the value of

the applied magnetic field according to Eq. (30), and choosing $R_0/R_c = \alpha_{s1}/\alpha_{0n}$, the TE mode growth rate can be maximized for magnetic harmonic number s , thereby optimizing the microwave power output for radiation with frequency $\omega \approx s\omega_{cb}$.

ACKNOWLEDGMENTS

This research was supported by the National Science Foundation. The research by one of the authors (H.U.) was supported in part by the Office of Naval Research under the auspices of the University of Maryland-Naval Research Laboratory Joint Program in Plasma Physics.

REFERENCES

1. R. C. Davidson and C. D. Striffler, J. Plasma Physics 12, 353 (1974).
2. J. L. Hirshfield, I. B. Bernstein, and J. M. Wachtel, IEEE J. Quantum Electronics, Vol. QE-1, 237 (1965).
3. M. Friedman, D. A. Hammer, W. M. Manheimer, and P. Sprangle, Phys. Rev. Lett. 31, 753 (1973).
4. N. I. Zaytsev, T. B. Pankratova, M. I. Petelin, and V. A. Flyagin, Radio Engineering and Electronic Physics 19, 103 (1974).
5. D. V. Kisel, G. S. Korablev, V. G. Navelyeu, M. I. Petelin, and Sh. E. Tsimring, Radio Engineering and Electronic Physics 19, 95 (1974).
6. E. Ott and W. M. Manheimer, IEEE Trans. PS-3, 1 (1975).
7. P. Sprangle and W. M. Manheimer, Phys. Fluids 18, 224 (1975).
8. P. Sprangle and A. Drobot, IEEE Trans. MTT-25, 528 (1977).
9. K. R. Chu and J. L. Hirshfield, Phys. Fluids, in press (1978).
10. H. Uhm, R. C. Davidson, and K. R. Chu, "Self-Consistent Theory of Cyclotron Maser Instability for Intense Hollow Electron Beam", submitted for publication (1978).
11. I. S. Gradshteyn and I. M. Ryzhik, Table of Integrals and Series and Products (Academic Press, New York, 1965) Ch. 8.

FIGURE CAPTIONS

- Fig. 1 Equilibrium configuration and coordinate system.
- Fig. 2 Electron density profile [Eq. (13)].
- Fig. 3 The straight lines $\omega = kv_b + s\omega_c/\gamma_b$ and $\omega = kc/\beta_b$ intersect at $(\omega_0, k_0) = (s\omega_c\gamma_b, s\omega_c\gamma_b/c)$. For the TE mode, the curve $\omega = (k^2c^2 + \alpha_{0n}^2c^2/R_c^2)^{1/2}$ passes through (ω_0, k_0) provided $\alpha_{0n}c/R_c = s\omega_c$. For the TM mode, the curve $\omega = (k^2c^2 + \beta_{0n}^2c^2/R_c^2)^{1/2}$ passes through (ω_0, k_0) provided $\beta_{0n}c/R_c = s\omega_c$.
- Fig. 4 Electron orbit in a plane perpendicular to the z-axis.
- Fig. 5 Plots of (a) normalized TE mode growth rate $\gamma_b\omega_i/\omega_c$, and (b) normalized Doppler shifted real frequency $\text{Re}(\gamma_b\Omega_1/\omega_c) = [\gamma_b(\omega_r - kv_b) - \omega_c]/\omega_c$ versus R_0/R_c [Eq. (48)] for $s=1$, $\nu=0.001$, $\beta_0=0.4$, $\beta_b=0.286$ and several values of n .
- Fig. 6 Plots of normalized TM mode growth rate $\gamma_b\omega_i/\omega_c$ versus R_0/R_c [Eq. (51)] for parameters identical to Fig. 5.
- Fig. 7 Plots of normalized TE mode growth rate $\gamma_b\omega_i/\omega_c$ versus R_0/R_c [Eq. (48)] for (a) $s=2$, and (b) $s=3$, and parameters otherwise identical to Fig. 5.
- Fig. 8 Plots of (a) normalized maximum growth rate $(\gamma_b\omega_i/\omega_c)_m$, and (b) normalized Doppler shifted real frequency $\text{Re}(\gamma_b\Omega/\omega_c)$ versus β_0 , for $n=2$, $\nu=0.001$, $\beta_b=\beta_0/1.4$ and several values of s . The solid and broken curves correspond to the TE and TM modes, respectively.

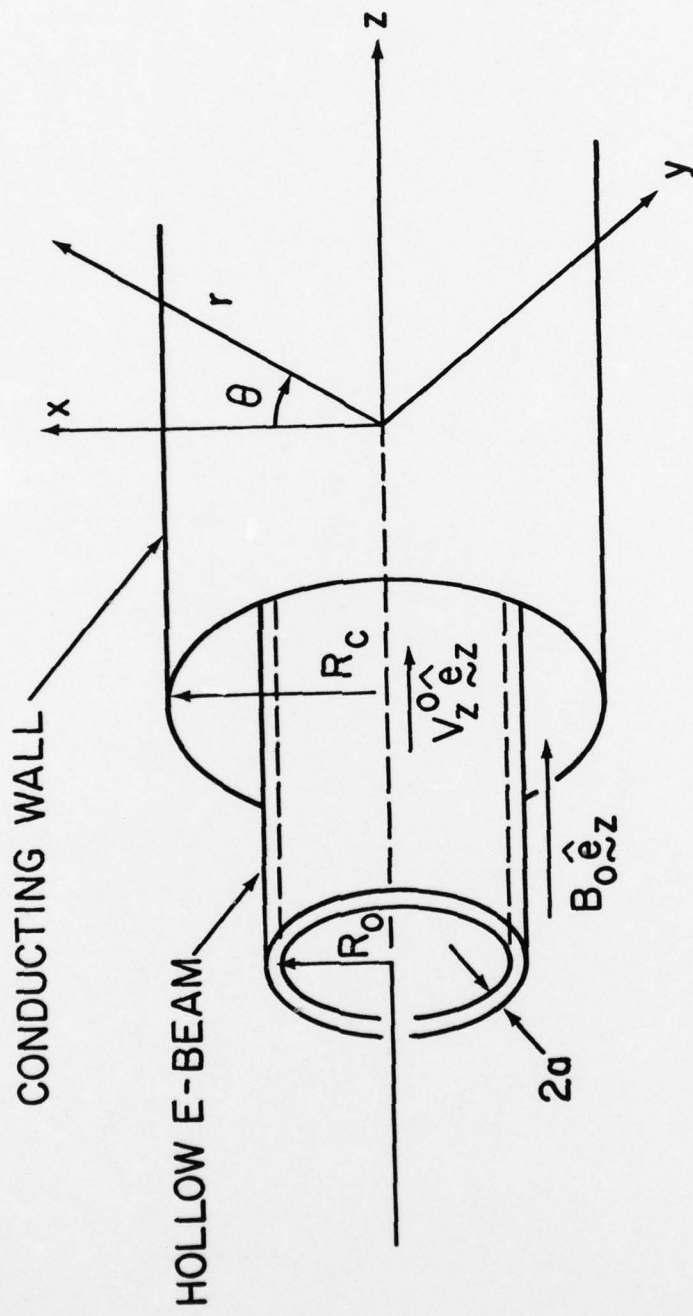


Fig. 1

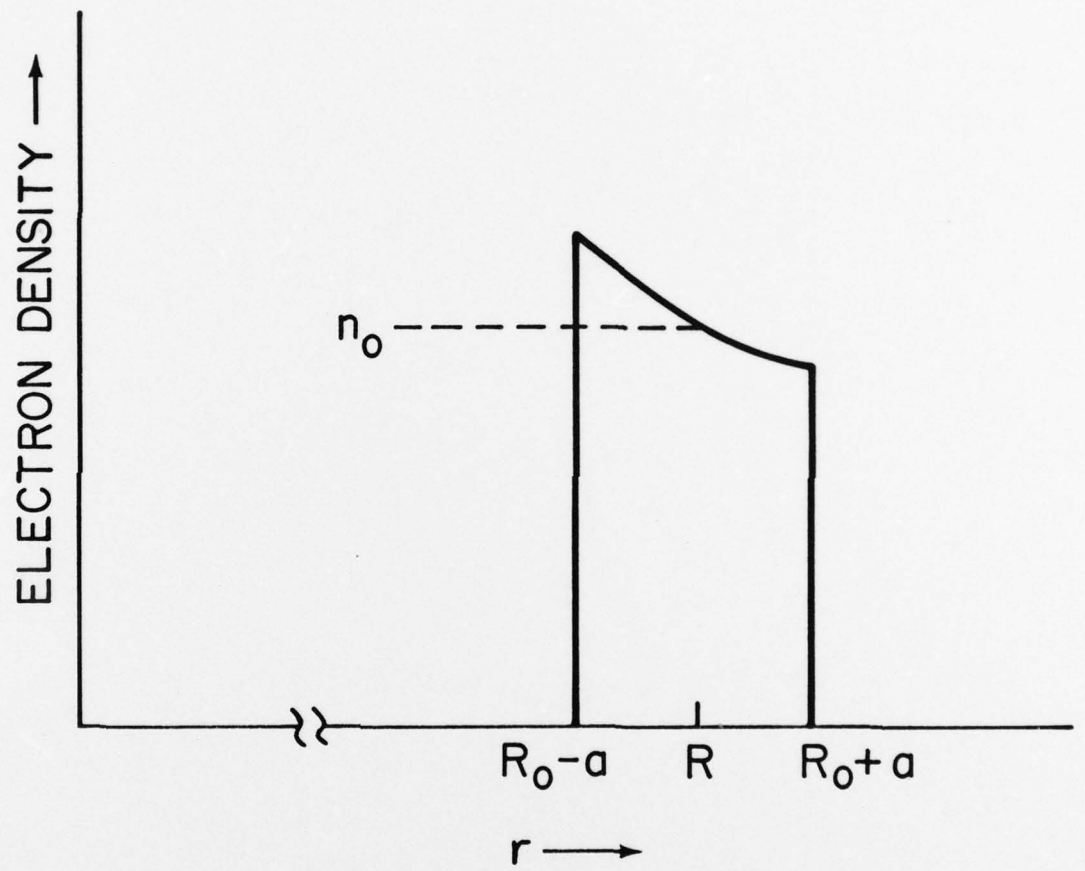


Fig. 2

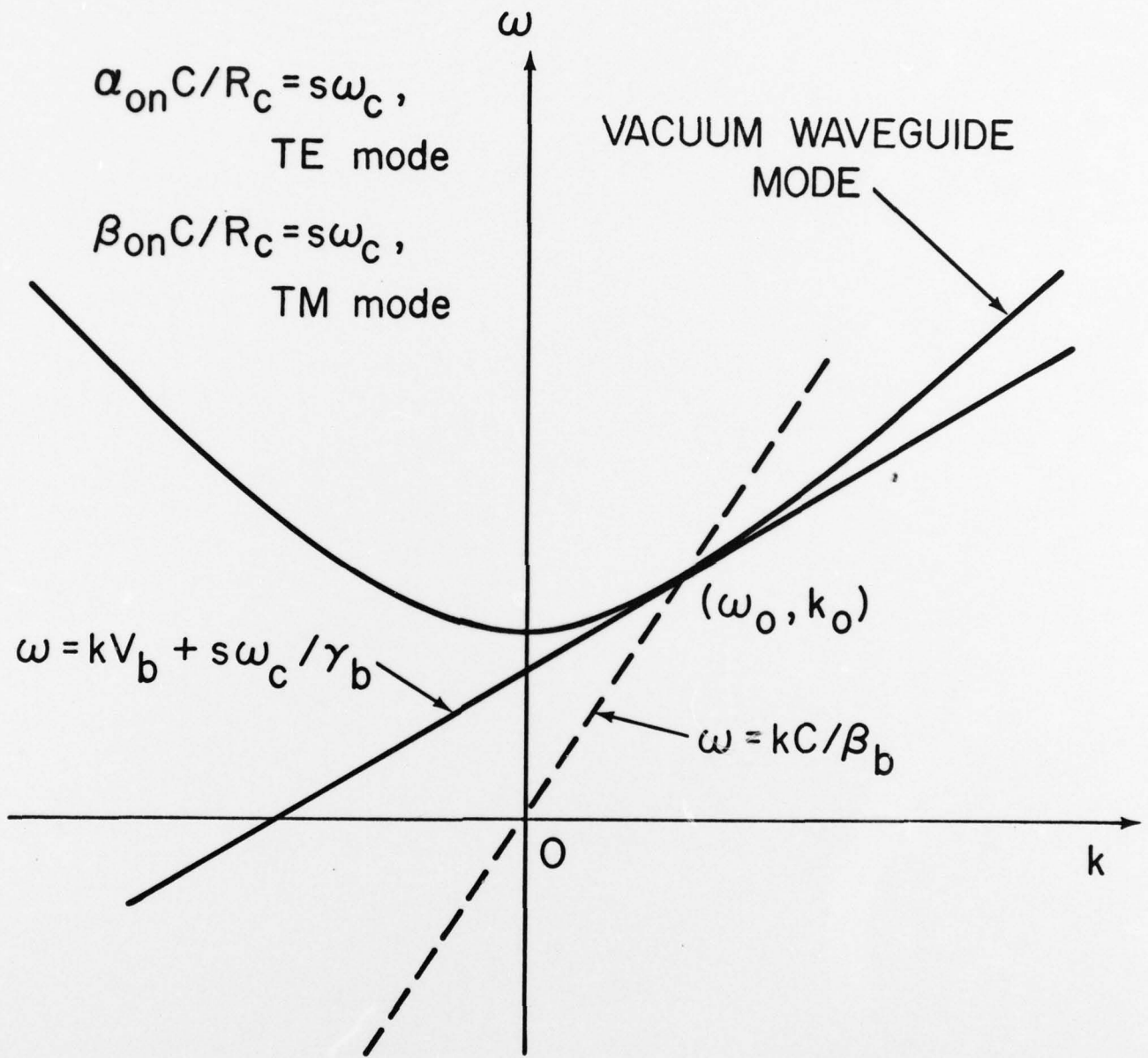


Fig. 3

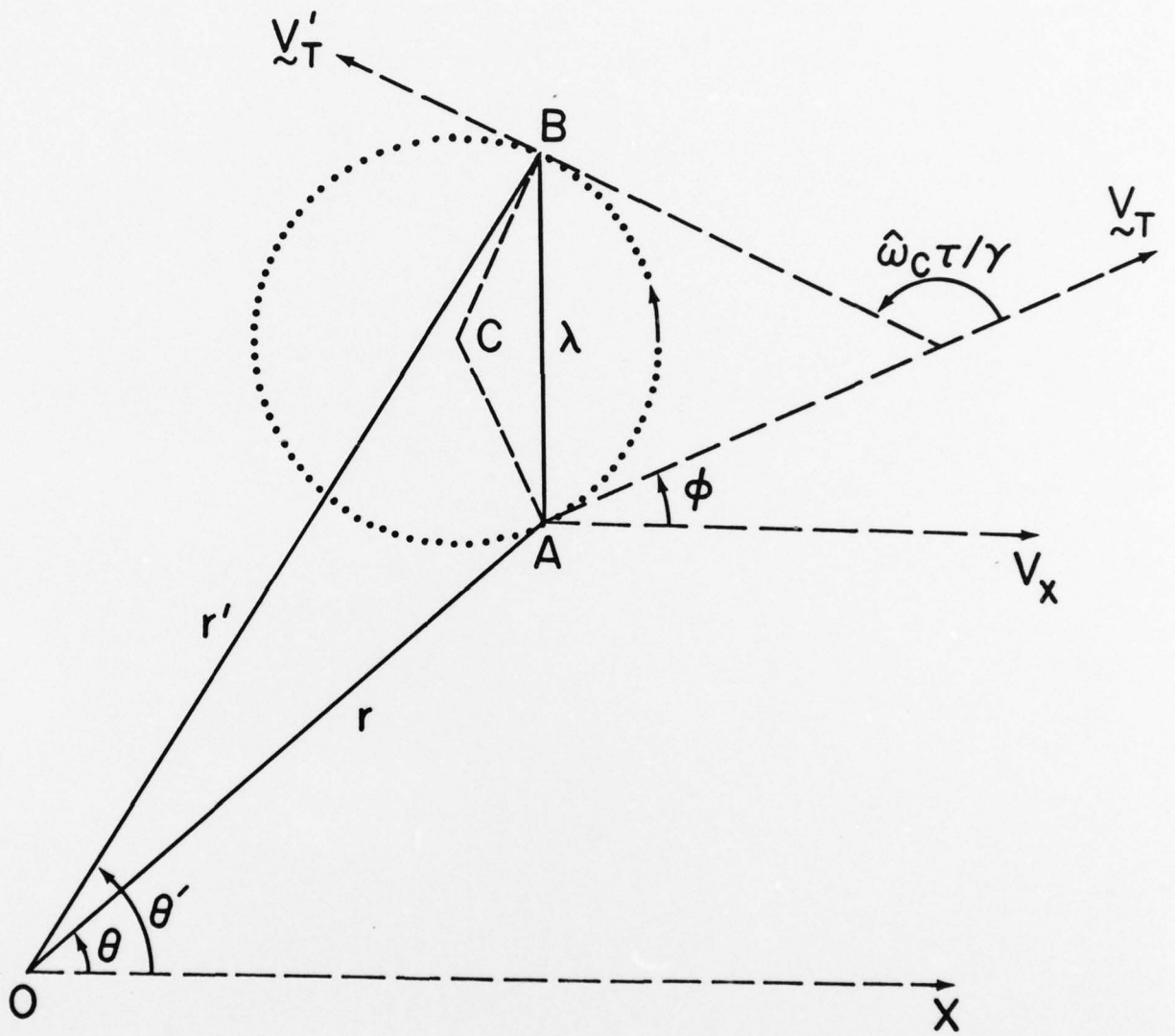


Fig. 4

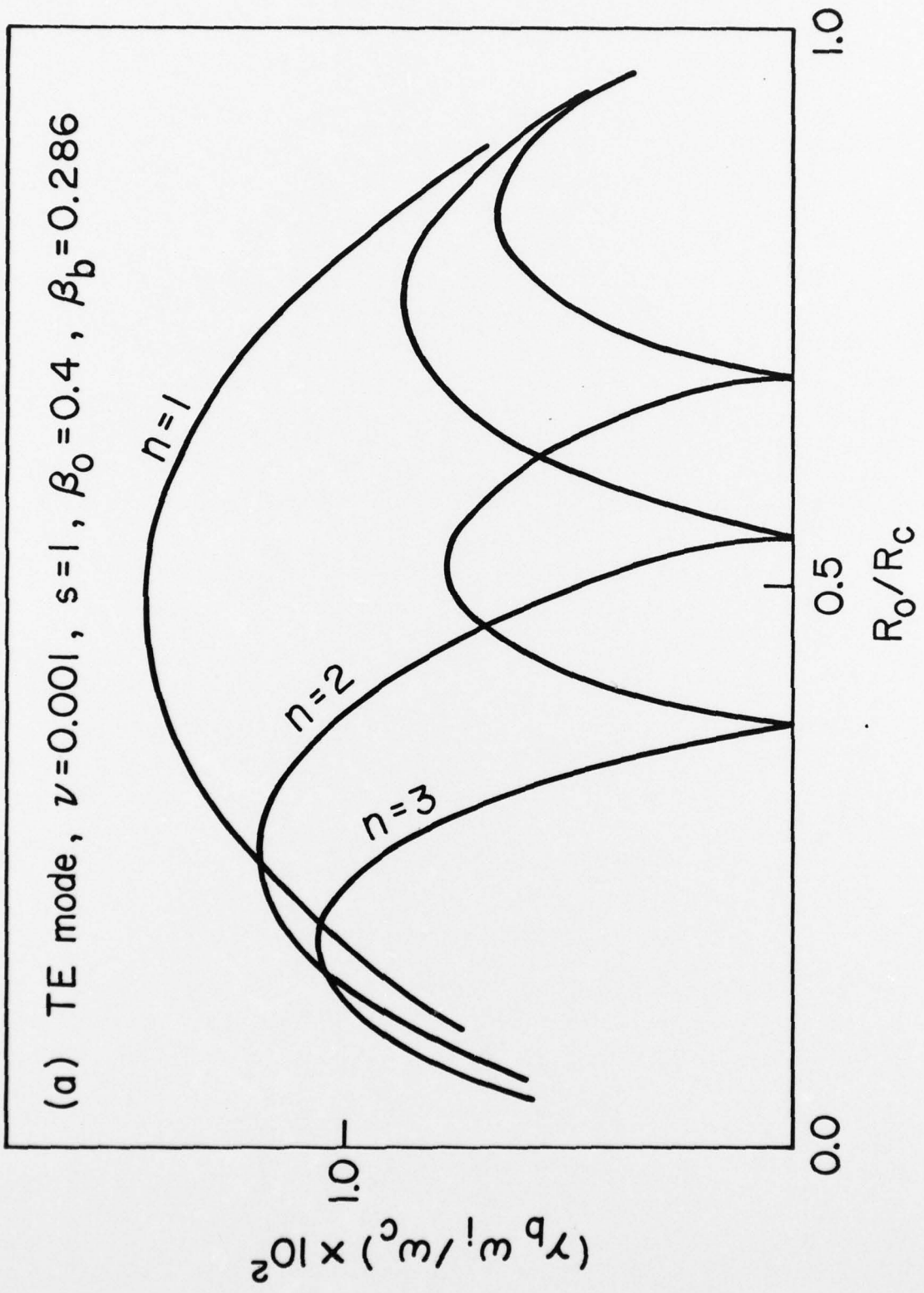


Fig. 5a

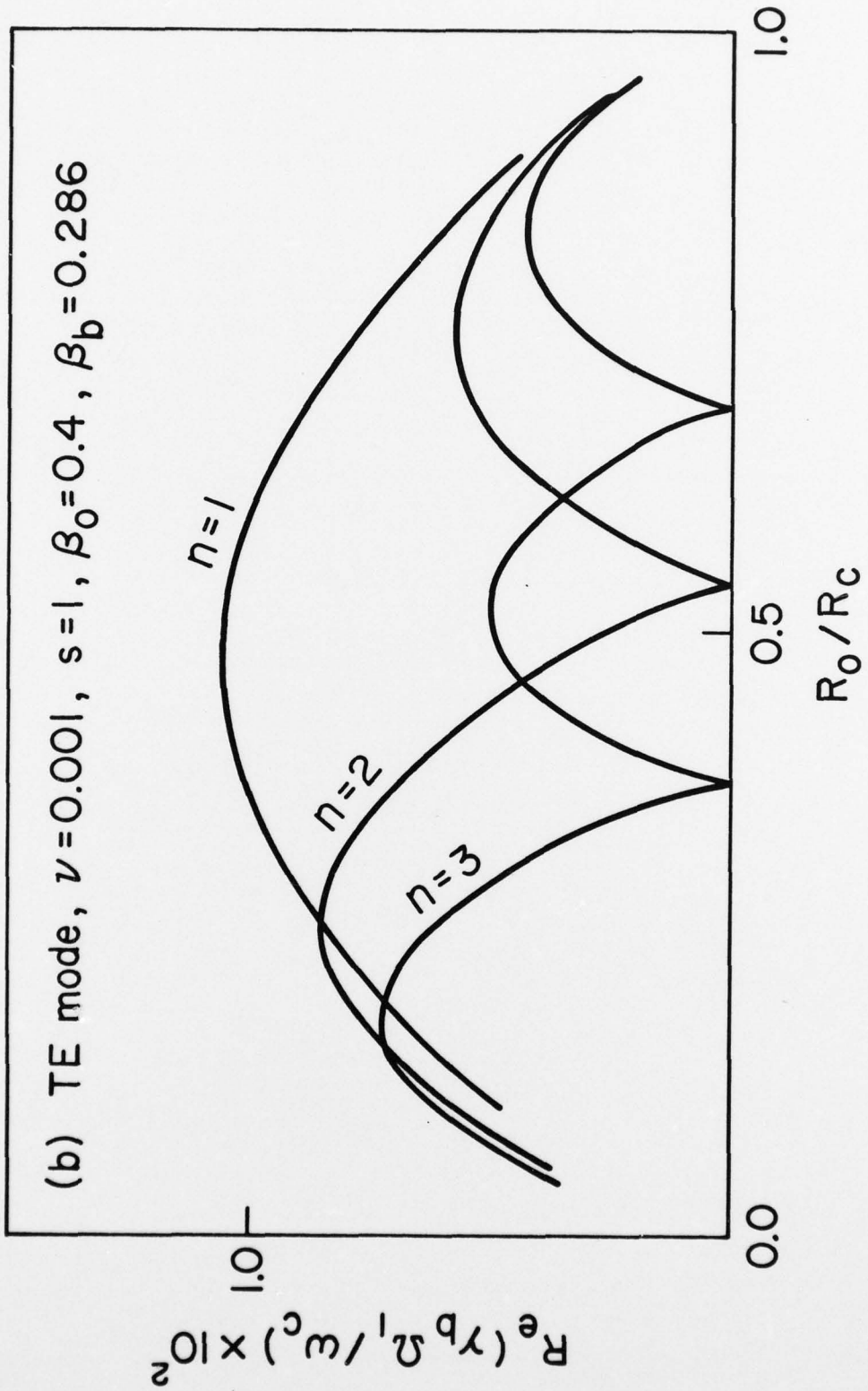


Fig. 5b

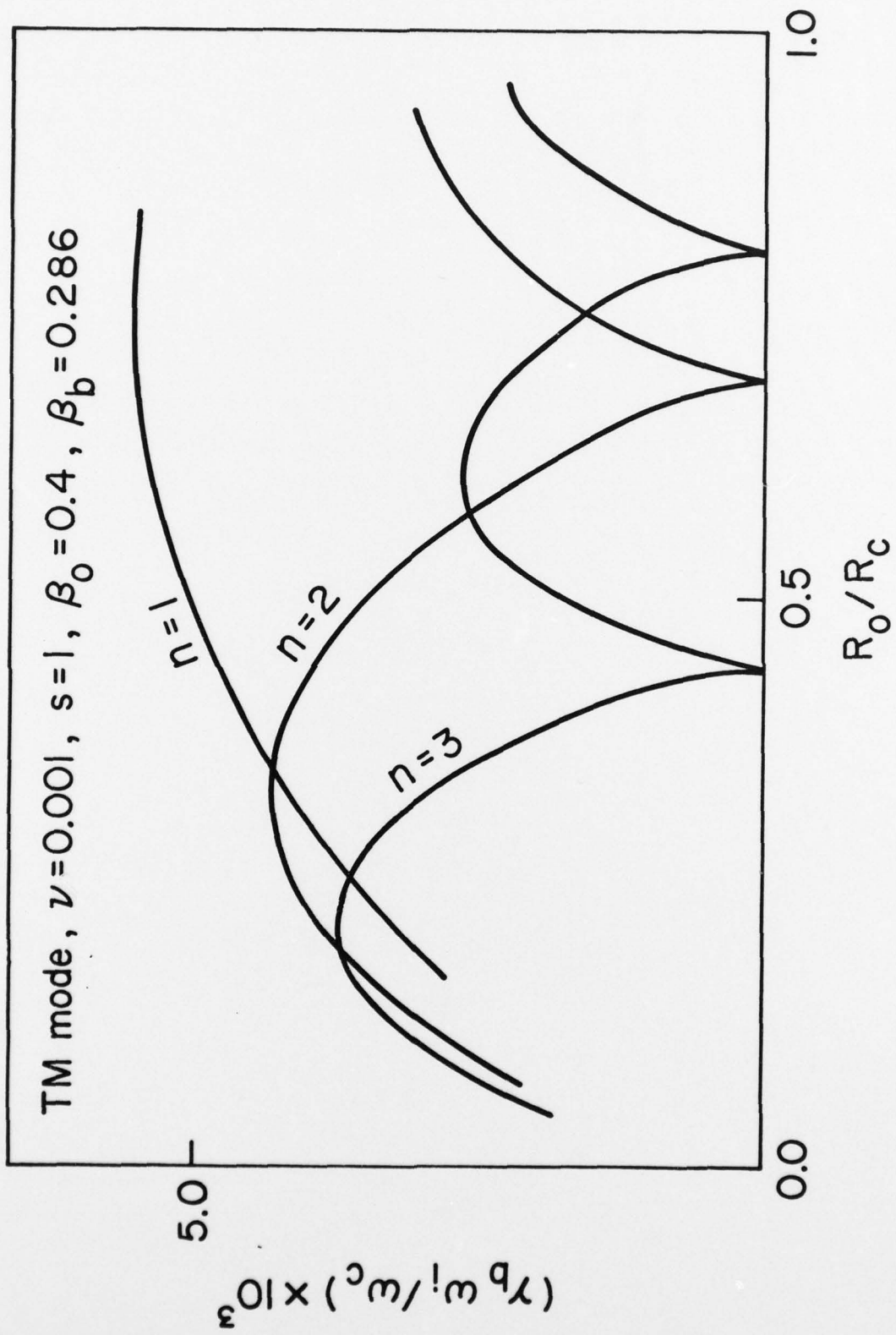


Fig. 6

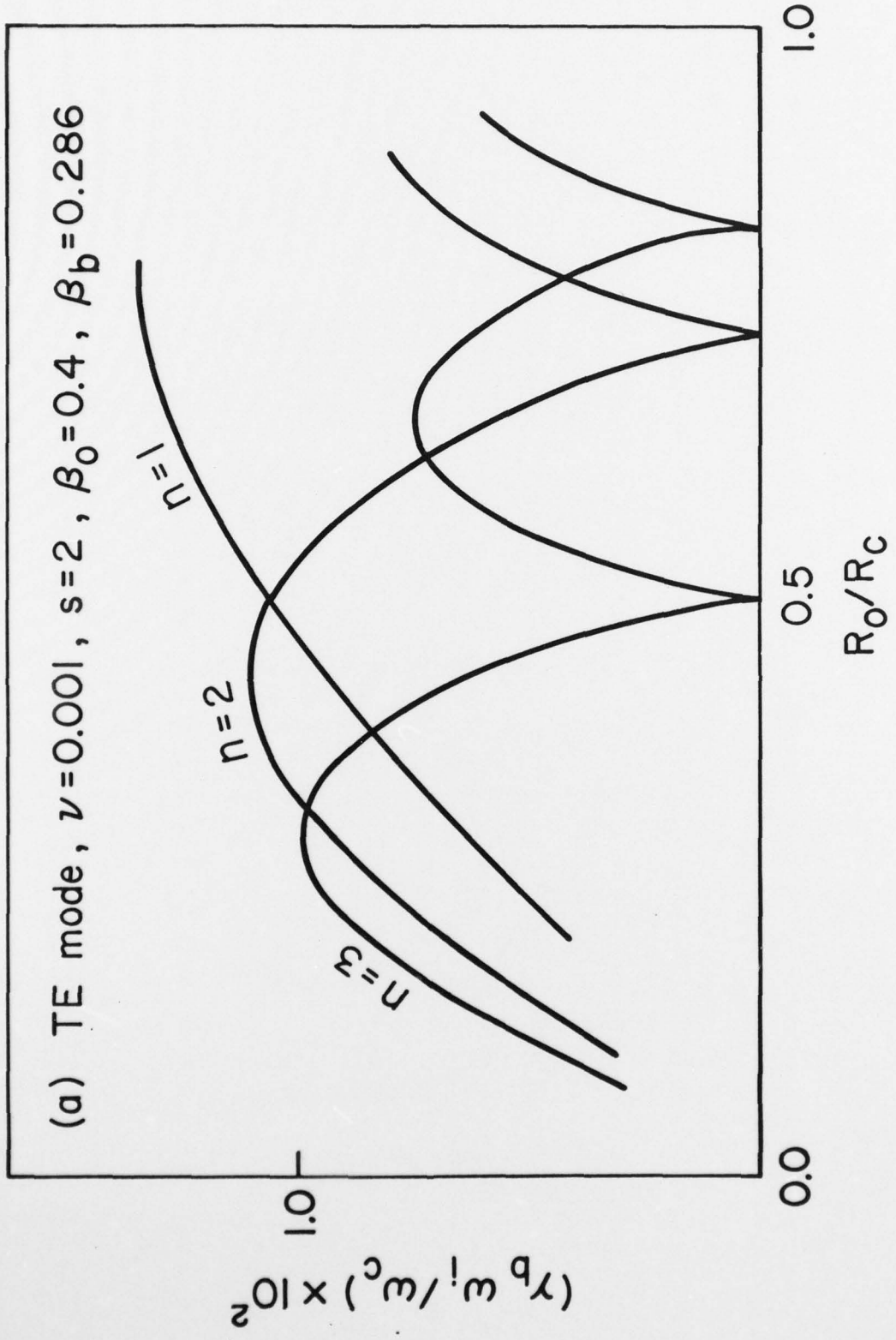


Fig. 7a

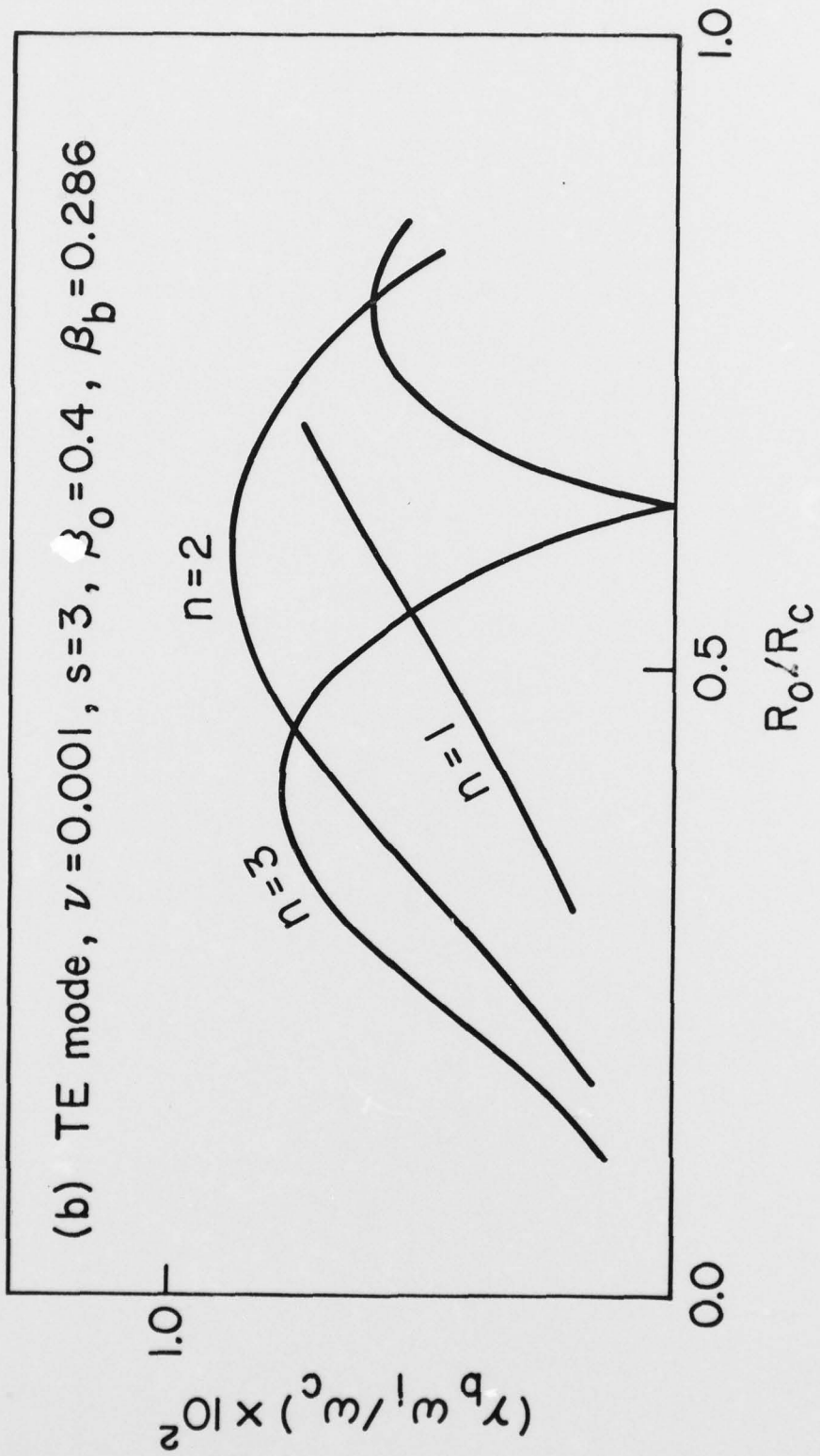


Fig. 7b

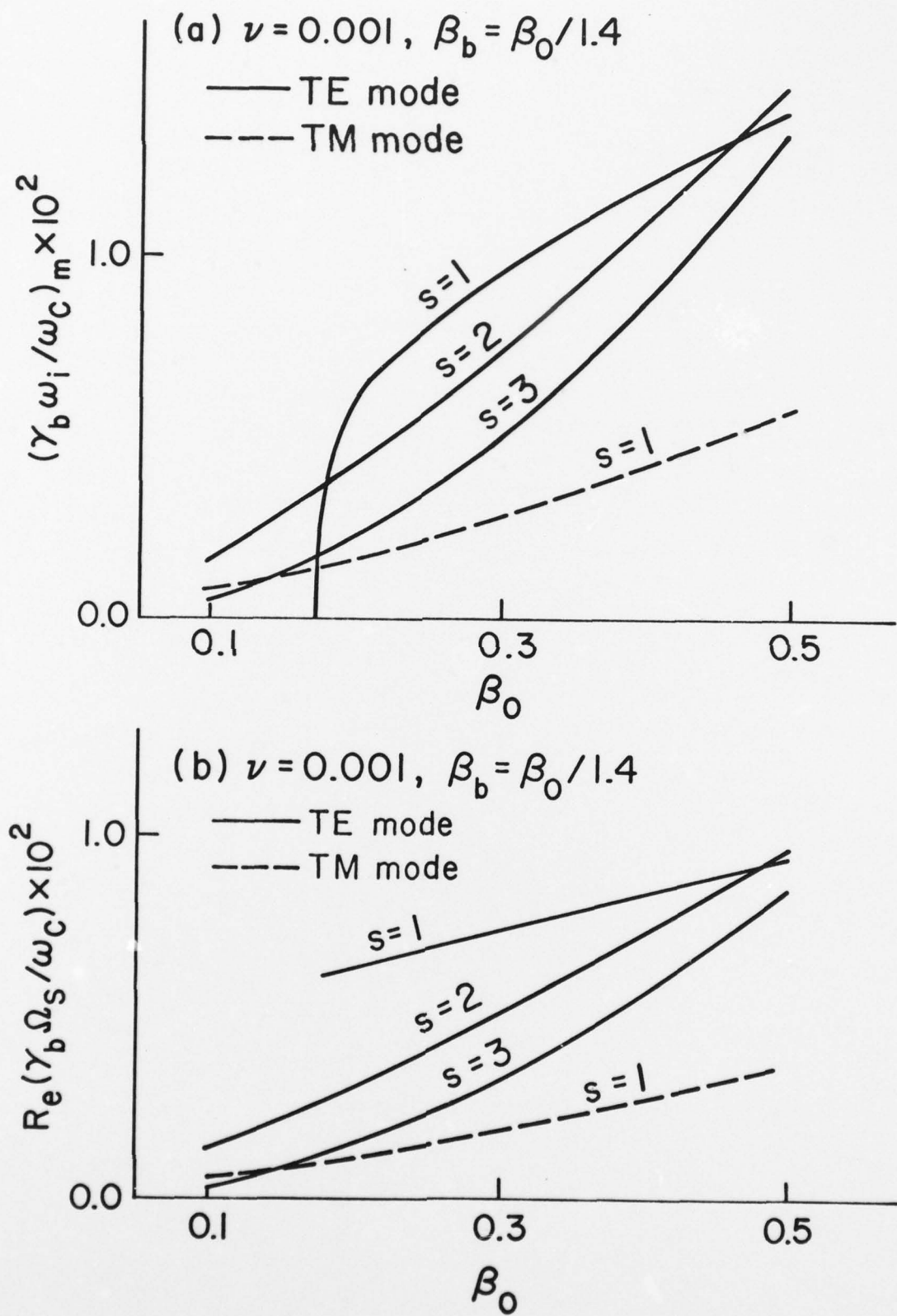


Fig. 8